Lattice dynamics and electron-phonon coupling in Sr_2RuO_4: Inelastic neutron scattering and shell-model calculations

M. Braden,[1,*] W. Reichardt,[2] Y. Sidis,[3] Z. Mao,[4] and Y. Maeno[5]
[1]*II. Physikalisches Institut, Universität zu Köln, Zülpicher Strasse 77, D-50937 Köln, Germany*
[2]*Forschungszentrum Karlsruhe, Institut für Festkörperphysik, P.O. Box 3640, D-76021 Karlsruhe, Germany*
[3]*Laboratoire Léon Brillouin, CEA/CNRS, F-91191 Gif-sur-Yvette Cedex, France*
[4]*Department of Physics, Tulane University, New Orleans, Louisiana 70118, USA*
[5]*Department of Physics, Kyoto University, Kyoto 606-8502, Japan*
(Received 13 February 2007; published 11 July 2007)

The lattice dynamics in Sr_2RuO_4 has been studied by inelastic neutron scattering combined with shell-model calculations. The in-plane bond-stretching modes in Sr_2RuO_4 exhibit a normal dispersion in contrast to all electronically doped perovskites studied so far. Evidence for strong electron phonon coupling is found for *c*-polarized phonons suggesting a close connection with the anomalous *c*-axis charge transport in Sr_2RuO_4. The role of this electron-phonon coupling in the superconducting pairing remains, however, a challenging open issue.

DOI: 10.1103/PhysRevB.76.014505 PACS number(s): 74.70.Pq, 74.25.Kc, 63.20.Kr

I. INTRODUCTION

The discovery of superconductivity in Sr_2RuO_4 (Ref. 1) has attracted attention partially due to the structural similarity with the high-temperature superconducting cuprates. Superconductivity in Sr_2RuO_4 is unconventional in character: from Knight-shift, μSR, and polarized neutron studies a triplet pairing was deduced.[2] Recently, direct evidence for an odd pairing symmetry was obtained by experiments on quantum interference devices[3] and by magneto-otpical Kerr effect.[4] In view of the unconventional pairing symmetry, the conventional electron-phonon coupling can be discarded from the possible pairing mechanisms, however, one may not rule out some exotic electron-lattice mechanism playing an important role. Indeed, the superconducting transition in Sr_2RuO_4 exhibits a remarkable isotope effect.[5] A detailed study of the lattice dynamics in this material appears hence highly desirable.

The lattice dynamics in Sr_2RuO_4 merits further interest as a reference material for the large class of transition metal-oxides with a perovskite related structure where an anomalous phonon dispersion has been observed.[6–21] Stimulated by the phenomenon of high-temperature superconductivity the phonon dispersion of many oxide perovskites has been studied in detail. In general the lattice dynamics of these materials is well understood with the aid of ionic lattice-dynamical models.[22,23] In particular in insulating parent compounds, such as La_2CuO_4, all features in the phonon dispersion are at least qualitatively described by simple ionic models. In electronically doped materials, such as $(La,Sr)_2CuO_4$, however, significant discrepancies in the dispersion of the longitudinal bond-stretching branches were discovered.[6–21] A typical lattice dynamical model including an isotropic screening function will always predict an increasing bond-stretching dispersion when passing from the Brillouin-zone center into the zone due to the imperfect screening of the Coulomb potentials at short distance. Instead a decreasing dispersion with the longitudinal zone-boundary frequencies falling below those of the transverse branch has been observed in numerous perovskite materials: in different types of superconducting cuprates,[6–15] in nickelates,[16,17] in manganates,[18] and in superconducting $Ba_{1-x}K_xBiO_3$,[19–21] for a recent review of these effects see Ref. 15. These doping-induced effects are frequently called over-screening[24] referring to the fact that simple screening should soften the longitudinal phonon modes. All these materials, however, are poor metals and they are all close to a charge ordering instability.[25] One may, hence, consider the frequency softening in the bond-stretching dispersion as a dynamic precursor of the charge ordering. Charge ordering at the metal site will modulate the bond distances to the O surroundings.[26] Therefore, charge ordering and the bond-stretching phonons are intimately coupled. For instance in the cuprates, the propagation vector where static stripe ordering is observed upon Nd codoping agrees well with the **q** vector of the anomaly in the longitudinal bond stretching branch.[8] A pronounced anomaly has recently been observed in materials passing into the charge-ordered stripe phase.[27]

As all the electronically doped oxide perovskites studied so far exhibit an anomalous bond-stretching dispersion, one may ask whether the over-screening effect should be considered as being anomalous. The study of additional materials is hence needed.

We have studied the phonon dispersion in Sr_2RuO_4 by inelastic neutron scattering and we have modeled it with ionic shell models taking the screening of the Coulomb potentials into account. The over-screening effect in the in-plane longitudinal bond-stretching dispersion is not found in Sr_2RuO_4 which is the only metallic oxide perovskite exhibiting a normal bond-stretching dispersion. However, the interplane charge dynamics seems to induce a pronounced softening of the *c*-axis polarized bond-stretching modes which must be taken as evidence for a strong-electron phonon coupling in this unconventional superconductor.

II. EXPERIMENTAL

The single crystals studied in this study were grown by the floating-zone technique[28] and these and crystals grown in

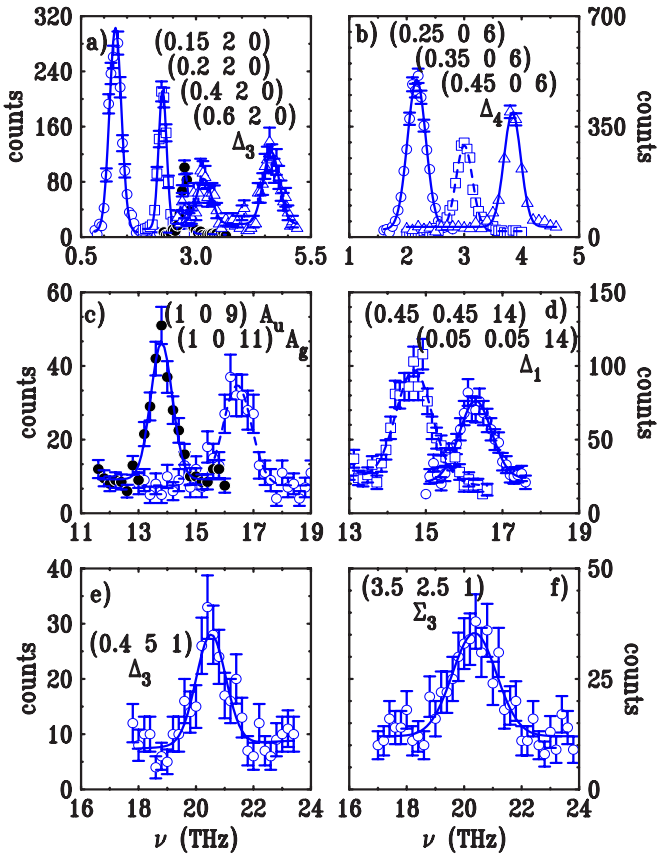

FIG. 1. (Color online) Typical scans to determine the phonon dispersion in Sr_2RuO_4. In parts (a) and (b) transverse acoustic phonon modes of Δ_3 and Δ_4 symmetry are shown, respectively. In part (c) scans across the two *c*-polarized apical-oxygen modes A_u and A_g are presented. At the A_g mode a Δ_1 branch starts for which part (d) shows two corresponding scans. In parts (e) and (f) scans across transverse in-plane bond-stretching modes are shown: (e) for a transverse mode along the [100] direction and (f) for the zone-boundary mode in [110] direction which is the quadrupolar mode.

the same way were already used in numerous inelastic neutron-scattering experiments aiming at the magnetic excitations in Sr_2RuO_4 (Refs. 29 and 30) as well as in many other studies.[2] Measurements were performed on the 1 T thermal triple-axis spectrometer at the Orphée reactor in Saclay. In the standard configuration we have used a pyrolithic graphite (PG) (002)-Bragg reflection monochromator at low energies (up to ~10 THz energy transfer) and a Cu-(111) monochromator at high energy. In order to suppress higher-order contaminations we have set a PG filter into the scattered beam and fixed the final energy to 3.55 or 7.37 THz (corresponding to 14.7 and 30.5 meV). The crystals were cooled to about 15 K with the aid of a closed-cycle cryostat. Most of the measurements were taken at that temperature. In order to study specific temperature dependencies a helium cryofurnace was used.

Typical scans aiming at phonons at quite different energies are shown in Fig. 1 covering the full energy range of the phonon dispersion in Sr_2RuO_4. In an inelastic neutron scattering experiment the scattering intensity I arising from a one-phonon process in neutron-energy loss mode is given by[31]

$$I \propto \frac{1}{\omega}[n(\omega)+1]\left\{\sum_d \frac{b_d}{\sqrt{m_d}} e^{(-W_d+i\mathbf{Q}\cdot\mathbf{r}_d)}(\mathbf{Q}\cdot\mathbf{e}_d)\right\}^2, \quad (1)$$

where ω denotes the phonon frequency ($\omega=2\pi\nu$, note that 1 THz corresponds to 4.14 meV), $\mathbf{q}$ the phonon wave vector, $\mathbf{Q}=\mathbf{g}+\mathbf{q}$ the scattering vector ($\mathbf{g}$ the reciprocal lattice vector), e^{-W_d} the Debye-Waller-factor, and the sum extends over the atoms in the primitive cell with mass m_d scattering length b_d, position $\mathbf{r}_d$ and polarization vector $\mathbf{e}_d$. In general, the intensity is determined by the Bose factor $n(\omega)$ and the $\frac{1}{\omega}$ term, which strongly reduce the effectiveness to observe high-energy modes. The dynamic structure factor equation (1) allows one to determine the full polarization of the modes by comparing the intensities measured in different Brillouin zones. In the other sense, a preliminary model may predict via Eq. (1) the favorable Brillouin-zones for the observation of particular phonon modes. Throughout this work we were guided by the lattice-dynamical model, which was successively improved with the growing amount of experimental information.

III. OVERALL PHONON DISPERSION AND LATTICE DYNAMICAL MODEL

Figure 2 shows the measured phonon dispersion together with the results of the lattice dynamical calculations. Sr_2RuO_4 crystallizes in the K_2NiF_4 structure in space group $I4/mmm$ with seven atoms in the primitive cell, accordingly the phonon dispersion consists of 21 phonon modes at the general position, but due to symmetry there are several degenerations at special points or lines. A small part of this data was already published earlier focusing on the lattice instability appearing at the zone boundary $\mathbf{M}=(0.5,0.5,0)$ of the Σ_3 branch.[32] The mode associated with the rotation of the RuO_6 octahedra around the *c* axis possesses a rather soft frequency as seen in the dip in the Σ_3 dispersion at the *M* point (0.5,0.5,0) and this mode exhibits an anomalous temperature dependency as reported in our first publication.[32] These effects must be considered as a precursor of the structural phase transition lowering the space-group symmetry from $I4/mmm$ to $I4_1/acd$ which has been observed in the meanwhile in the $Ca_{2-x}Sr_xRuO_4$ series.[33,34] In contrast to the rotational mode, the octahedron-tilting mode does not show anomalous effects in Sr_2RuO_4. This dynamic precursor of the rotational instability is perfectly described by the lattice-dynamics model.

In a first approach, one may attribute the branches in the range of 4 THz to Sr/Ru vibrations and those in the range 5–12 THz to different Ru and Ru-O bond-bending modes. The modes in the frequency range 14–16 Thz correspond to vibrations of the apical oxygen parallel to the *c* axis and the highest band of phonons with frequencies above 20 THz is associated with the in-plane bond-stretching vibrations. Only three zone-center modes are Raman active and were observed by Udagawa *et al.*[35,36] The two A_g modes corresponding to the *c*-axis vibrations of Sr and to that of the apical oxygen are found at 5.96 and 16.49 THz, respectively, and one E_g mode is found at 7.36 THz.[35,36] The corresponding frequencies determined by inelastic neutron scattering per-

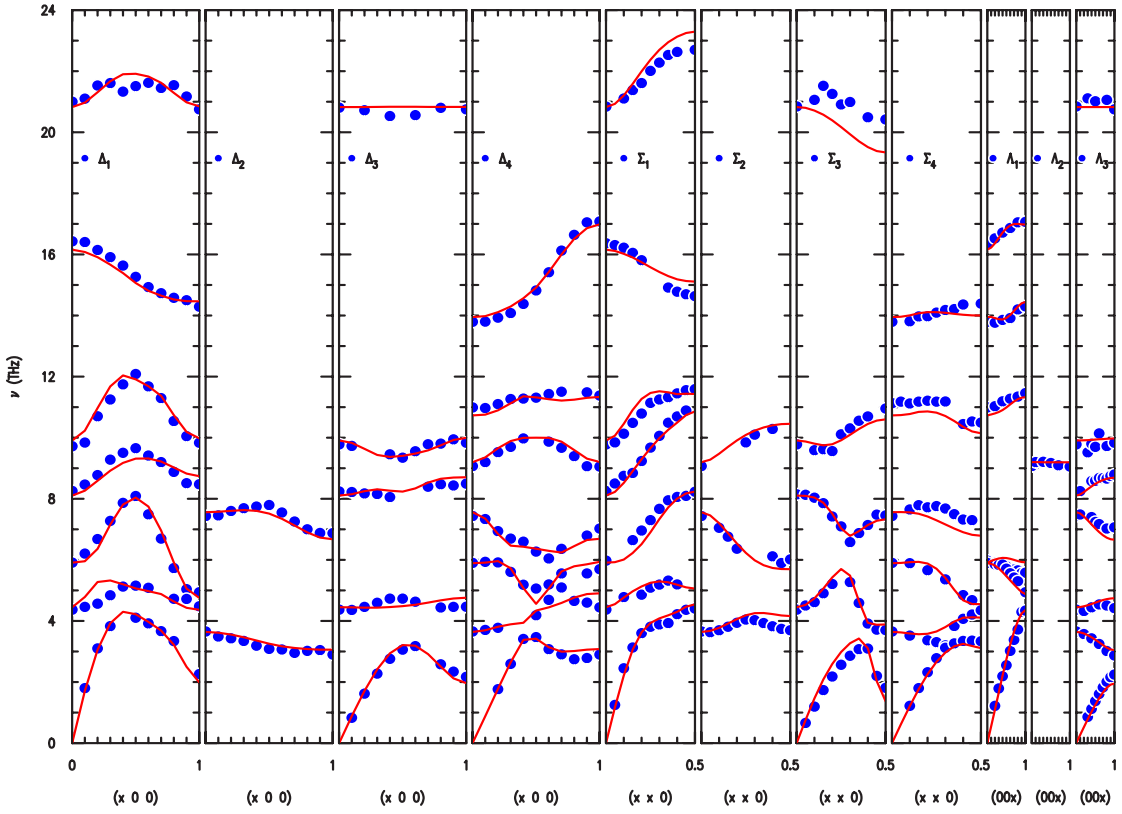

FIG. 2. (Color online) Phonon dispersion in Sr_2RuO_4, symbols denote the measured frequencies and lines those calculated with the lattice dynamical model. We show the phonon dispersion along the main symmetry directions [100], [110], and [001], separated according to the irreducible representations, see text and Table I.

fectly agree with these Raman results, we find the frequencies 6.02, 16.44, and 7.27 THz. Due to the good in-plane electrical conductivity, infrared optical measurements with the polarization parallel to the planes were unable to observe any phonon modes but the three c-polarized A_u frequencies at 5.92, 11.11, and 14.49 THz have been determined.[37] The two lower frequencies agree well with our results giving 5.94 and 10.99 THz. However, we find the highest A_u mode at 13.80 THz. Since the determination of the phonon frequencies has not been the focus of the infrared study, no raw-data were shown in Ref. 37 and we cannot further comment on the high-frequency discrepancy.

The 21 modes at the zone center can be separated according to the irreducible representations into one B_u (observed at 9.09 THz), two A_g (6.02 and 16.44 THz), four A_u (5.94, 10.99 and 13.80 THz plus acoustic mode), two double-degenerated E_g (3.59 and 7.27 THz), and five double-degenerated E_u (4.38, 8.36, 9.72, and 20.85 THz and acoustic mode). Along the main-symmetry directions [100] (Δ), [110] (Σ), and [001] (Λ) the modes can be separated according to three or four irreducible representations. In our notations the subscript 1 always refers to the representation the longitudinal acoustic mode belongs to. Subscript 2 signifies the representation which does not contain any acoustic mode, and subscripts 3 and 4 (the latter is not used for Λ modes) denote the representations containing the transverse acoustic modes with c-polarized acoustic modes belonging to representation 4. The polarization schemes and the compatibility relations of the irreducible representations are given in Table I.

We have tried to describe the observed phonon dispersion of Sr_2RuO_4 in a Born–von Karman force-constant model taking into account atomic pairs up to 15th shell or 30 parameters. For a metallic material one may expect such a model to yield a good description. In Sr_2RuO_4 there are clear discrepancies, for example the relatively large elastic constants compared to the lower zone-boundary frequencies, which suggest the relevance of long-range interactions arising from Coulomb potentials. We, therefore, have modeled the phonon dispersion of Sr_2RuO_4 in an ionic shell model, whose parameters are given in Table II. Starting from the generalized model presented in Ref. 22 we have adapted the parameters to the measured dispersion under the additional constraint of the resulting forces not getting too large.

For the description of the phonon dispersion in Sr_2RuO_4 we use Coulomb potentials with effective charges $V(r) \propto Z_1 Z_2 e^2/r$ and the repulsive forces are described by Born-Mayer potentials $V(r)=A\exp(-r/r_0)$. Shell charges describing a single-ion polarizability have been introduced for all atoms with shell-core force constants chosen anisotropic for Sr and Ru. The interatomic forces act on the shells in our model. We treat the in-plane oxygen (O1) and the apical oxygen (O2) differently, similar to the case of the cuprates, but the same O-O potential was used for all pairs. For the O-O-interaction we have added a van der Waals term of $-100(\text{ev Å}^6)r^{-6}$ with r the interatomic distance in Å. All cal-

TABLE I. Upper part: Polarization schemes according to the crystal structure of Sr_2RuO_4 for all Γ modes and for the representations along the [100], [110], and [001] directions (labeled Δ, Σ, and Λ, respectively); the first line gives the positions of seven atoms forming a primitive unit (Ref. 38), the following lines show the displacements of these atoms. A letter at the i position, signifies that this atom is moving along the i direction, a second appearance of the same letter signifies that the second atom moves with the same amplitude ("−" denotes a phase shift) in the corresponding direction. Lower part: Compatibility relations of the irreducible representations for phonon wave vectors along the main-symmetry directions.

	Sr 0 0 0.0353	Sr′ 0 0 −0.353	Ru 0 0 0	O1 0.5 0 0	O1′ 0 0.5 0	O2 0 0 0.162	O2′ 0 0 −0.162
1 B_u	0 0 0	0 0 0	0 0 0	0 0 *A*	0 0 −*A*	0 0 0	0 0 0
2 A_g	0 0 *A*	0 0 −*A*	0 0 0	0 0 0	0 0 0	0 0 *B*	0 0 −*B*
4 A_u	0 0 *A*	0 0 *A*	0 0 *B*	0 0 *C*	0 0 *C*	0 0 *D*	0 0 *D*
2 E_g	*A* 0 0	−*A* 0 0	0 0 0	0 0 0	0 0 0	*B* 0 0	−*B* 0 0
5 E_u	*A* 0 0	*A* 0 0	*B* 0 0	*C* 0 0	*D* 0 0	*E* 0 0	*E* 0 0
7 Δ_1	*A* 0 *B*	*A* 0 −*B*	*C* 0 0	*D* 0 0	*E* 0 0	*F* 0 *G*	*F* 0 −*G*
2 Δ_2	0 *A* 0	0 −*A* 0	0 0 0	0 0 0	0 0 0	0 *B* 0	0 −*B* 0
5 Δ_3	0 *A* 0	0 *A* 0	0 *B* 0	0 *C* 0	0 *D* 0	0 *E* 0	0 *E* 0
7 Δ_4	*A* 0 *B*	−*A* 0 *B*	0 0 *C*	0 0 *D*	0 0 *E*	*F* 0 *G*	−*F* 0 G
7 Σ_1	*A A B*	*A A* −*B*	*C C* 0	*D E* 0	*E D* 0	*F F G*	*F F* −*G*
3 Σ_2	*A* −*A* 0	−*A A* 0	0 0 0	0 0 *B*	0 0 −*B*	*C* −*C* 0	−C *C* 0
5 Σ_3	*A* −*A* 0	*A* −*A* 0	*B* −*B* 0	*C D* 0	−*D* −*C* 0	*E* −*E* 0	*E* −*E* 0
6 Σ_4	*A A B*	−*A* −*A* B	0 0 *C*	0 0 *D*	0 0 *D*	*E* −*E* F	−*E* E F
6 Λ_1	0 0 *A*	0 0 *B*	0 0 *C*	0 0 *D*	0 0 *D*	0 0 *E*	0 0 *F*
1 Λ_2	0 0 0	0 0 0	0 0 0	0 0 *A*	0 0 −*A*	0 0 0	0 0 0
7 Λ_3	*A* 0 0	*B* 0 0	*C* 0 0	*D* 0 0	*E* 0 0	*F* 0 0	*G* 0 0
[100]	Δ_1:2 A_g+5 E_u			Δ_2:2 E_g			
	Δ_3:5E_u			Δ_4:1 B_u+2E_g+4A_u			
[110]	Σ_1:2A_g+5 E_u			Σ_2:1 B_u+2E_g			
	Σ_3:5 E_u			Σ_4:2E_g+4A_u			
[001]	Λ_1:2 A_g+4 A_u			Λ_2:1 B_u			
	2·Λ_3:2 E_g+5 E_u						

culations were performed with the GENAX program.[39]

In addition to the potentials a few additional force constants were introduced to improve the description. Angular forces were added for the linear O1-Ru-O1 and O2-Ru-O2 bonds and special force constants were needed in order to describe the behavior of the c-polarized bond-stretching modes, as it will be discussed below.

IV. SOFT ROTATIONAL MODE

Since our first report on the softening of the rotational mode in Sr_2RuO_4 the structural studies on the phase diagram of $Ca_{2-x}Sr_xRuO_4$ have shown the close connection between the static octahedron rotation and the electronic and magnetic properties in $Ca_{2-x}Sr_xRuO_4$.[33,34] Therefore, it appeared interesting to study the temperature dependence of the rotational mode in more detail in Sr_2RuO_4 which, however, does not exhibit the static distortion.[38] The new results on the rotational mode confirm our previous measurement and are given in Fig. 3. The rotational mode was measured at $\mathbf{Q}=(2.5,1.5,0)$ in the [100],[010] scattering geometry. Between the lowest and the highest temperature (~450 K) the rotational mode continuously broadens whereas the frequency first softens up to about room temperature and then stiffens upon further temperature increase. These temperature dependencies cannot be explained by a normal structural instability where the mode should soften and broaden concomitantly. Instead, we think that these anomalous effects have to be attributed to electron-phonon coupling. The strongest temperature effects in both, in the frequency and in the width, are observed near 150 K, where the c-axis resistivity exhibits a broad maximum. The anomalous temperature dependency of the rotational mode might thus be connected with the c-axis charge transport.

V. SCREENING OF COULOMB POTENTIALS BY CHARGE CARRIERS

The metallic character of Sr_2RuO_4 yields an effective screening of the Coulomb potentials and was explicitly taken

TABLE II. Lattice dynamics model parameters for the description of the phonon dispersion in Sr_2RuO_4; for the explanation of the parameters see text; Z,Y are given in electron charges; K in 10^6 dyn/cm.

ionic part			
ion	Z	Y	K
Ru	2.58	0.47	8.0/2.0
Sr	2.00	5.86	3.6
O1	−1.52	−3.25	1.8
O2	−1.77	−2.77	1.8

potentials			
pair	A (eV)	r_0 (Å)	C (eV/Å^6)
Sr-O1	1825	0.318	
Sr-O2	2250	0.318	
Ru-O1	2999	0.260	
Ru-O2	3874	0.260	
O1-O1	2000	0.284	−100
O1-O2	2000	0.284	−100
O2-O2	2000	0.284	−100

additional force constants (dyn/cm)	
constant	F
angular O1-Ru-O1	6798
angular O2-Ru-O2	11178
special O2-z	3205
special breathing	−5203

into account in the lattice-dynamics calculations. We describe the electronic susceptibility by the Lindhard function for a free-electron gas.[22] In such model the screening is perfect at long distance, thereby the splitting between longitudinal optic (LO) and transverse optic (TO) phonon frequencies disappears at the Brillouin-zone center. However, when passing into the zone, the screening will be less effective as it has to occur at shorter distance and the LO-TO splitting may partially recover yielding an increasing dispersion close to the zone center. The screening scenario applies to any polar modes, in particular to those with Ru-O bond-bending character, which posses the strongest polar character in Sr_2RuO_4. Since in other perovskites these bending modes are associated with ferroelectricity, they are frequently called ferroelectric modes. Comparison of the Sr_2RuO_4 low-temperature phonon dispersion with those observed in $La_{1.85}Sr_{0.15}CuO_4$ (Ref. 22) and in $Nd_{1.85}Ce_{0.15}CuO_4$ (Ref. 15) immediately reveals differences. The bond-bending branches in the ruthenate are much flatter indicating a more effective screening. The relevant Δ_1 and Σ_1 branches starting at the E_u mode at 9.72 THz attain only frequencies of about 12 THz in the ruthenate whereas they exhibit a steep dispersion up to 16 THz in the cuprates starting at a comparable zone-center frequency. Also along the c direction the screening is rather perfect in Sr_2RuO_4, as the Λ_1 branch starting at the 11 THz A_u mode is rather flat. The comparably efficient screening perpendicular to the planes is further corroborated by the

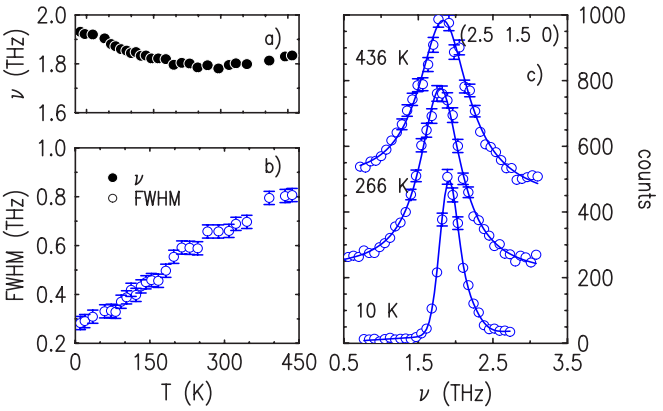

FIG. 3. (Color online) Temperature dependence of the rotational mode in Sr_2RuO_4, (a) mode frequency and (b) width. The mode was measured at $\mathbf{Q}=(2.5,1.5,0)$ in the [100], [010] scattering geometry. Raw-data scans at three temperature are shown in part (c), these scans were fitted by Lorentzian profiles in order to obtain the positions and widths (for the 10 K scan a second Lorentzian is used to take into account a resolution effect).

model calculations where an isotropic screening formalism is found to describe the dispersion relation reasonably well. The isotropic screening contrasts with the anisotropic transport properties of Sr_2RuO_4, where resistivity ratios $\frac{\rho_c}{\rho_{\text{inplane}}}$ of the order of 1000 were reported.[40,41]

In the case of Sr_2RuO_4 we obtain a screening vector of $k_s=0.86$ Å^{-1} which is considerably larger than the one found, for example in $La_{2-x}Sr_xCuO_4$, $k_s=0.39$ Å^{-1} for $x\sim 0.1$ (Ref. 22) or the one observed in $Nd_{2-x}Ce_xCuO_4$ $k_s=0.41$ Å^{-1} for $x=0.15$.[15] Qualitatively, the efficient screening agrees with the better metallic properties of the ruthenate. Using a screening vector of $k_s=0.42$ Å^{-1}, similar to those observed in the cuprates, we find also a comparable phonon dispersion. The longitudinal branches starting at the ferroelectric bond-bending modes are then found to attain frequencies of 16 THz for propagation vectors along and perpendicular to the planes as it is indeed observed in the cuprates.

At low temperature, Sr_2RuO_4 exhibits a considerably higher in-plane electrical conductivity than the cuprates. However, upon heating the conductivity considerably decreases in Sr_2RuO_4 attaining values at high temperature which are comparable to those observed in the cuprates. The in-plane mean free path in Sr_2RuO_4 was reported to fall below 1 Å without any sign for resistivity saturation upon heating up to 1200 K.[41] One may, therefore, wonder, whether the efficient low-temperature screening in Sr_2RuO_4 is significantly reduced upon heating as well. To study this problem we have analyzed the ferroelectric bond-bending modes at different temperatures for the Δ_1 and Λ_1 branches. However, all temperature-induced phonon-frequency shifts are very small, of the order of one percent, whereas an essential change of the screening rendering the ruthenate at room temperature comparable to the cuprates would imply frequency shifts by more than 30%. We may conclude that the high screening of the Coulomb potentials in Sr_2RuO_4 remains essentially unchanged between 10 K and room temperature. The screening of Coulomb potentials seems to be fully de-

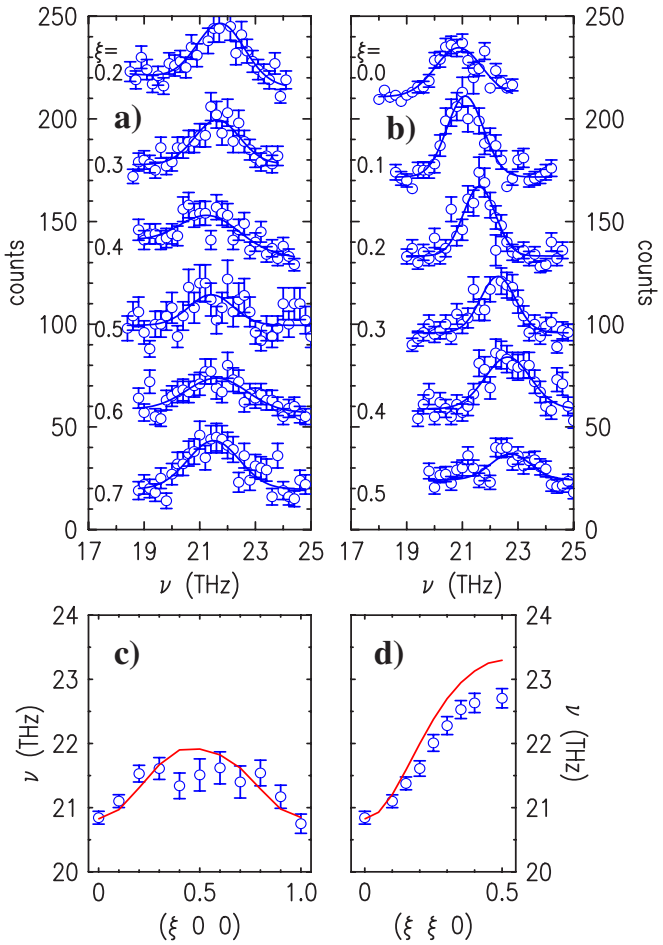

FIG. 4. (Color online) Raw data scans to determine the longitudinal bond-stretching modes at $\mathbf{q}=(\xi,0,0)$ (a) and at $(\xi,\xi,0)$ (b), for clarity scans were successively translated vertically. Dispersion of the in-plane bond-stretching phonon modes along the [100] (c) and [110] direction (d); symbols denote the measured frequencies and lines the dispersion calculated with the lattice dynamics model.

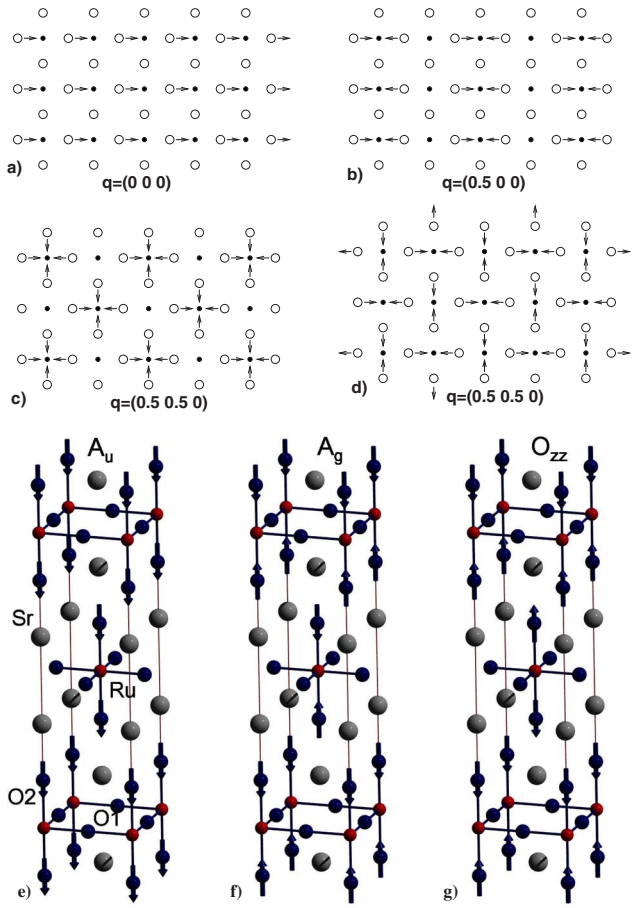

FIG. 5. (Color online) Polarization patterns of several bond-stretching modes. Parts (a), (b), and (c) display the elongations within a single RuO_2 layer for the longitudinal in-plane bond-stretching modes at the zone center, at $\mathbf{q}=(0.5,0,0)$ (half-breathing mode) and at $\mathbf{q}=(0.5,0.5,0)$ (planar beathing mode), respectively. Part (d) shows the polarization pattern of the transverse bond-stretching mode at $\mathbf{q}=(0.5,0.5,0)$ of quadrupolar character. Three z-polarized bond-stretching mode patterns are given in parts (e)–(g): the A_u (e) and the A_g (f) modes at the Brillouin-zone center and the O_{zz} mode at the **Z** point (g).

coupled from the macroscopic charge transport.

Qualitatively the minor temperature-induced frequency changes agree with a very small reduction of the screening upon heating; the zone-center modes slightly soften (E_u) or remain unchanged (A_u) whereas there is a minor hardening for polar modes in the Brillouin zone upon heating, but none of these effects is stronger than 2%.

VI. DISPERSION OF BOND-STRETCHING MODES

The dispersion of the in-plane bond-stretching modes is shown in detail in Fig. 4. Starting at the highest E_u frequency a Δ_1 branch connects to the half-breathing mode at $\mathbf{q}=(0.5,0,0)$ and then continues to the $\mathbf{Z}=(1,0,0)$ point bond-stretching mode with an out-of-phase vibration of neighboring planes. For the corresponding polarization patterns see Figs. 5(a) and 5(b). Unfortunately, there is a strong loss in the dynamical structure factor when approaching the half-breathing mode rendering these measurements always difficult. The raw data shown in Fig. 4(a), however, document that the branch can be followed along this path by combining measurements in different Brillouin zones, mostly (4,0,0), (5,1,0), and (5,0,3). This branch shows a rather flat dispersion and a nearly **q**-independent width. There is no over-screening effect along the [100] direction comparable to those observed in all metallic perovskites observed so far. The dispersion is reasonably well described by our lattice-dynamical model, see Fig. 4(c).

Also along the [110] direction, we do not find the over-screening effect but a rather normal and increasing dispersion towards the planar breathing mode at $\mathbf{q}=(0.5,0.5,0)$, for the polarization pattern see Fig. 5(c). Figure 4(b) shows the scans taken most at $\mathbf{Q}=(3+\xi,3+\xi,2)$ and in Fig. 4(d) the dispersion is presented, which again is well reproduced by the shell model.

The normal bond-stretching dispersion contrasts with all electronically doped perovskite compounds studied so far, as all of them exhibit a pronounced over-screening effect at

least along one of the in-plane directions. The difference between Sr_2RuO_4 and the materials studied previously consists in the fact that Sr_2RuO_4 is intrinsically metallic implying a relatively higher charge carrier density. More importantly, it appears that the charge carriers in Sr_2RuO_4 possess a higher mobility. Sr_2RuO_4 exhibits a low residual resistivity and well-defined Fermi-liquid behavior at low temperatures.[2] The ruthenate does not seem to be close to any charge-ordering instability with an inhomogeneous distribution of charges within the RuO_2 layers.

The debate about the role of electron-phonon coupling in cuprate high-temperature superconductivity has gained further weight with the interpretation that the kink observed in angle resolved photoemission spectroscopy (ARPES) spectra of many high-temperature superconducting compounds arises from electron-phonon coupling.[42] This interpretation contrasts with the explanation given by other groups, who attribute the kink to an interaction with magnetic excitations.[43] A comparable kink has more recently been found in the ARPES spectra of Sr_2RuO_4 as well.[44,45] Therefore, the comparison of the lattice dynamics of this material with that of the cuprates might help understanding the origin of these kinks. In view of the absence of the corresponding phonon anomaly in the in-plane bond-stretching dispersion of the ruthenate it appears rather unlikely that these in-plane bond-stretching modes are essential for the understanding of the ARPES kinks. The multi-band Fermi surface in Sr_2RuO_4 renders the comparison with the cuprates more complex, but the kinks in Sr_2RuO_4 have been attributed to the d_{xy} band[45] which is the one most similar to the cuprate $d_{x^2-y^2}$ band. The ARPES kinks in the ruthenate could arise from magnetic excitations as Sr_2RuO_4 exhibits magnetic fluctuations of nearly antiferromagnetic character and of comparable strength as those in cuprates.[29,30,46]

Figures 5(e)–5(g) show the polarization patterns of different out-of-plane bond-stretching modes. At the zone-center there is an odd A_u and an even A_g mode where the two O2's connected to a Ru-site vibrate in and out-of-phase, respectively. Due to the translation symmetry, the octahedron at the center of the tetragonal cell moves in phase with the one at the origin for the zone-center modes. For $\mathbf{q}$ at the point $\mathbf{Z}=(1,0,0)$, however, the two octahedra vibrate with opposite phases, see Fig. 5. The A_g mode connects with the so-called O_{zz} mode at $\mathbf{Z}$ through a Δ_1 branch and the A_u mode to its analog through a Δ_4 branch. The O_{zz} mode is interesting in terms of a possible coupling with charge fluctuations. At the same time all oxygens connected to a certain Ru-layer move towards that layer whereas those O2's connected to the neighboring layers move away from those. This mode may, hence, be considered as the c-axis polarized analog of the linear breathing mode; it can be coupled with an interlayer charge transfer.[47,48]

Basing on a simple ionic lattice dynamical model one expects roughly similar frequencies for the A_g and the O_{zz} modes. However, we find a steep downwards dispersion in the Δ_1 branch connecting these two modes, see Fig. 6. From the A_g frequency at 16.4 THz the frequencies of the branch decrease towards the value of 14.5 THz observed for the O_{zz} mode. Two scans across this branch are shown in Fig. 1(d). In contrast the Δ_4 branch exhibits an increasing dispersion

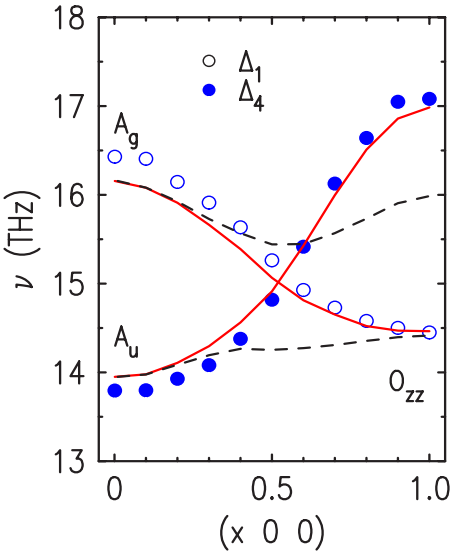

FIG. 6. (Color online) Dispersion of the z-polarized bond-stretching phonons along the [100] direction; the A_g/O_{zz} and $A_u/\mathbf{Z}$-A_u modes connect through Δ_1 and Δ_4 branches, respectively. The broken lines give the results of a normal lattice dynamics model which is unable to describe the dispersion properly. The solid lines correspond to the dispersion calculated with the inclusion of the special force constants.

from the A_u mode towards the corresponding $\mathbf{Z}$-point mode. This dispersion cannot be described with the normal ionic model, the corresponding dispersion is indicated in Fig. 6 by the broken lines. In order to describe the pronounced softening of the O_{zz} mode without affecting the description of the other modes we had to introduce two specially adapted force constants, see Table I. The O_{zz} force constant acts on the two O2 sites connected to the same Ru, and the breathing constant chosen negative acts on the in-plane oxygens connected to the same Ru. These constants mimic the observed dispersion rather well but they do not possess an intrinsic physical meaning. With these additional parameters a good description of the bond-stretching dispersion is obtained except the transverse Σ_3 branch connecting to the quadrupolar mode at $\mathbf{q}=(0.5,0.5,0)$, see Fig. 1(f)) for a raw-data scan and Fig. 5(d) for the polarization pattern, where the model predicts a softening stronger than the one found experimentally.

We think that the anomalously soft O_{zz}-mode frequency has to be attributed to a strong electron-phonon coupling, as it is further supported by the temperature dependence. In two independent experiments we have studied the temperature dependence of these c-axis polarized Δ_1 modes between 15 and 300 K and between 15 and 450 K. The results are resumed in Fig. 7. The entire Δ_1 branch softens upon heating, but the softening is much stronger at the O_{zz} mode where it exceeds the expectation for a typical mode Grüneisen parameter, see Figs. 7(b) and 7(c). In addition, at room temperature the O_{zz} mode is significantly broader than the other modes studied in this branch. Most interestingly the anomalous softening of the O_{zz} mode occurs just above about ~150 K, which is the crossover temperature observed in the c axis electric resistivity.[40,41] Concomitantly, the width of the O_{zz} mode increases at this temperature range. The measurements

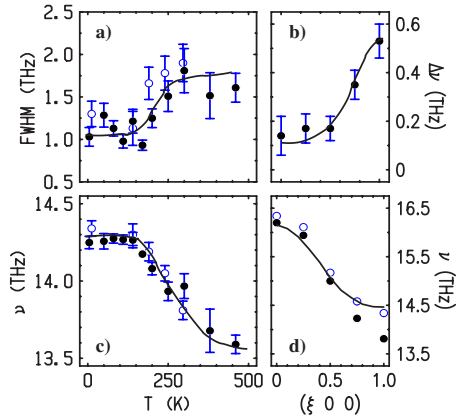

FIG. 7. (Color online) Temperature dependencies of peak widths and frequencies of the *c*-polarized bond-stretching Δ_1 modes. (a), (c) Temperature dependencies of the peak width (a) and of the frequency (c) of the O_{zz} mode, respectively. These results were determined in two independent experiments (open and filled symbols). (b), (d) **q** dependence of the temperature-induced frequency shifts (b) and of the phonon frequencies of this Δ_1 branch (d) at 15 K (open symbols) and at room temperature (filled symbols).

of the optical conductivity in Sr_2RuO_4 have revealed that the charge transport along the *c* direction is coherent only at low temperatures.[37]

We attribute the anomalous dispersion near the O_{zz} mode as well as the temperature effects to a strong coupling between this phonon mode and the interlayer charge transport. This electron lattice coupling causes considerable phonon softening and broadening in particular at high temperature where the charge transport is incoherent. Evidence for a much stronger electron-phonon coupling associated with the O_{zz} mode was found in the isostructural cuprate $(La,Sr)_2CuO_4$ (Ref. 7) and in less extent in $Nd_{1.85}Ce_{0.15}CuO_4$.[15] For the hole-doped cuprates, Falter *et al.* have explained the anomalous effects by a coupling with interlayer charge fluctuations.[47,48] Ho and Schofield have analyzed the temperature dependence of the anisotropic resistivity of a two-dimensional metal and in particular the existence of a resistivity maximum along the less coupled direction in terms of an anisotropic electron-boson coupling.[49] They obtained an excellent fit to the *c*-axis resistivity in Sr_2RuO_4 assuming the characteristic energy of the coupling boson at $k_B515\ \mathrm{K} \sim 11$ THz, which agrees reasonably well with the energy of the O_{zz} mode of 14 THz, corroborating the conclusion that strong electron-phonon coupling for the O_{zz} mode is associated with the uncommon *c*-axis charge transport.

Bands of different orbital character contribute to the Fermi surface in Sr_2RuO_4.[2] Amongst them, the d_{xz} and the d_{yz} states should be most relevant for the *c*-axis charge transport and also most sensitive to the strong coupling with the O_{zz} phonon mode. The electron-phonon coupling, thus, should be more important for these d_{xz} and d_{yz} states possibly competing with a nonconventional superconducting pairing mechanism. The anisotropic electron-phonon coupling in Sr_2RuO_4 might, therefore, enhance the orbital selective character of the superconductivity in Sr_2RuO_4.[50]

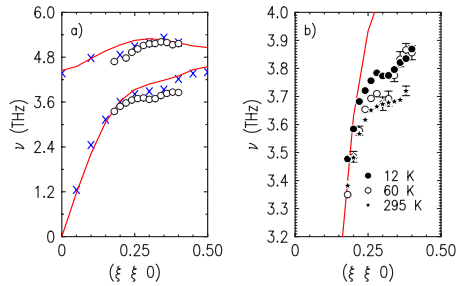

FIG. 8. (Color online) Dispersion of the longitudinal acoustic and the lowest optical branch of the same symmetry along the [110] direction, Σ_1 modes. In part (a) crosses denote the data taken to establish the overall dispersion shown in Fig. 2. Open circles denote the results of measurements at 60 K with the PG monochromator; filled circles and stars present the data obtained with the Cu-(111) monochromator achieving higher resolution. Lines correspond to the frequencies calculated with the lattice dynamical model.

VII. SEARCH FOR A KOHN-ANOMALY

Pure[29] and Ti-doped Sr_2RuO_4 (Ref. 51) are textbook examples for pronounced Fermi-surface nesting. The quasi-one-dimensional d_{xz} and d_{yz} bands form flat Fermi-surface sheets yielding strong nesting at the **q** position $(0.3,0.3,q_l)$. In pure Sr_2RuO_4 this nesting implies sharply peaked magnetic fluctuations[29,30,46] and upon minor Ti substitution a static spin-density wave develops at this propagation vector.[51] We have studied the question whether the pronounced peak in the electronic susceptibility yields a signature in the lattice dynamics as well which would correspond to a Kohn anomaly.

The longitudinal breathing modes along the [110] direction are a first promising candidate to search for a Kohn anomaly, since the breathing modes are intrinsically coupled with the Ru-site charges. In the in-plane bond stretching dispersion shown in Fig. 4, however, no such signature can be detected in spite of the high precision obtained for that branch. Another candidate for a Kohn anomaly is the longitudinal acoustic branch which belongs to the same Σ_1 representation. In order to detect such an anomaly we have measured the phonon frequencies in the lowest two Σ_1 branches with much higher precision than the data taken in order to establish the global dispersion in Fig. 2. At 60 K one data set was taken in the [100]/[010] scattering geometry using the PG monochromator. We also used the [110]/[001] scattering geometry in combination with the PG monochromator yielding comparable results but less precision due to the less favorable alignment of the resolution ellipsoid. Another data set was taken in [100]/[010] scattering using the Cu-(111) monochromator yielding a better energy resolution at 12 and 295 K. The results of these measurements are shown in Fig. 8. Indeed one may discern a small dip in the lowest branch just at $\mathbf{q}=(0.3,0.3,0)$ which is somehow smeared out at room temperature. This dip, however, is superposed with the effects arising from the anticrossing behavior of the two branches of the same symmetry which may explain the weak plateau in the acoustic branch around $\mathbf{q}=(0.25,0.25,0)$–$(0.35,0.35,0)$. Anyway the effect of the nesting has to be

considered as being weak. It appears very unlikely that such an electron phonon coupling is a relevant effect in Sr_2RuO_4.

VIII. CONCLUSIONS

The lattice dynamics of Sr_2RuO_4 in spite of its excellent metallic properties at low temperatures still shows the characteristic features of an ionic compound. The dispersion is best described in an ionic shell model taking account of the electronic screening. Compared to previously studied perovskites, in particular the high-temperature superconducting cuprates, the screening is more efficient in Sr_2RuO_4. There is no direct relation between the screening and electric transport properties, as, in contrast to the transport, the screening is isotropic and essentially temperature independent.

In view of the anomalous bond-stretching dispersion observed in all electronically doped perovskites studied so far, this aspect is particularly interesting in Sr_2RuO_4 as well. The in-plane bond-stretching dispersion, however, is rather normal in Sr_2RuO_4. The anomalous effects in the other materials may hence not simply be attributed to their metallic character. Instead it seems likely that the high mobility of the charge carriers along the planes in Sr_2RuO_4 inhibits the strong coupling between the breathing modes and charge fluctuations. The absence of the in-plane bond-stretching anomalies in Sr_2RuO_4 together with the observation of kinks in ARPES spectra resembling those of the cuprates, renders a dominant role of the in-plane bond-stretching phonons in the cuprate-kink mechanism unlikely.

A highly anomalous bond-stretching dispersion is, however, observed for the *c*-polarized bond-stretching modes in Sr_2RuO_4. The O_{zz} zone-boundary mode exhibits a rather low frequency and a strongly temperature-dependent line broadening. These effects indicate that this mode is coupled with the anomalous charge transport along the *c* direction observed in dc resistivity and in optical conductivity experiments. Whether this sizeable electron-phonon coupling plays some role in the superconducting pairing mechanism in Sr_2RuO_4, remains a challenging open issue.

ACKNOWLEDGMENTS

Work at Universität zu Köln was supported by the Deutsche Forschungsgemeinschaft through the Sonderforschungsbereich 608.

*Electronic address: braden@ph2.uni-koeln.de

[1] Y. Maeno, H. Hashimoto, K. Yoshida, S. Nishizaki, T. Fujita, J. G. Bednorz, and F. Lichtenberg, Nature (London) **372**, 532 (1994).
[2] A. P. Mackenzie and Y. Maeno, Rev. Mod. Phys. **75**, 657 (2003).
[3] K. D. Nelson, Z. Q. Mao, Y. Maeno, and Y. Liu, Science **306**, 1151 (2004).
[4] J. Xia, Y. Maeno, P. T. Beyersdorf, M. M. Fejer, and A. Kapitulnik, Phys. Rev. Lett. **97**, 167002 (2006).
[5] Z. Q. Mao, Y. Maeno, Y. Mori, S. Sakita, S. Nimori, and M. Udagawa, Phys. Rev. B **63**, 144514 (2003).
[6] B. Renker, F. Gompf, E. Gering, N. Nuecker, D. Ewert, W. Reichardt, and H. Rietschel, Z. Phys. B: Condens. Matter **67**, 15 (1987); B. Renker, F. Gompf, E. Gering, D. Ewert, H. Rietschel, and A. Dijanoux, *ibid.* **73** 309 (1988); B. Renker, F. Gompf, E. Gering, G. Roth, D. Ewert, H. Rietschel, and H. Mutka, *ibid.* **71**, 437 (1988).
[7] L. Pintschovius and W. Reichardt, in *Neutron Scattering in Layered Copper-Oxide Superconductors*, edited by A. Furrer, Vol. 20 of *Physics and Chemistry of Materials with Low-Dimensional Structures* (Kluwer Academic, Dordrecht, 1998), p. 165.
[8] L. Pintschovius and M. Braden, Phys. Rev. B **60**, R15039 (1999).
[9] R. J. McQueeney, Y. Petrov, T. Egami, M. Yethiraj, G. Shirane, and Y. Endoh, Phys. Rev. Lett. **82**, 628 (1999).
[10] R. J. McQueeney, J. L. Sarrao, P. G. Pagliuso, P. W. Stephens, and R. Osborn, Phys. Rev. Lett. **87**, 077001 (2001).
[11] W. Reichardt, J. Low Temp. Phys. **105**, 807 (1996).
[12] J.-H. Chung, T. Egami, R. J. McQueeney, M. Yethiraj, M. Arai, T. Yokoo, Y. Petrov, H. A. Mook, Y. Endoh, S. Tajima, C. Frost, and F. Dogan, Phys. Rev. B **67**, 014517 (2003).
[13] H. Uchiyama, A. Q. R. Baron, S. Tsutsui, Y. Tanaka, W.-Z. Hu, A. Yamamoto, S. Tajima, and Y. Endoh, Phys. Rev. Lett. **92**, 197005 (2004).
[14] M. d'Astuto, P. K. Mang, P. Giura, A. Shukla, P. Ghigna, A. Mirone, M. Braden, M. Greven, M. Krisch, and F. Sette, Phys. Rev. Lett. **88**, 167002 (2002).
[15] M. Braden, L. Pintschovius, T. Uefuji, and K. Yamada, Phys. Rev. B **72**, 184517 (2005).
[16] L. Pintschovius, W. Reichardt, M. Braden, G. Dhalenne, and A. Revcolevschi, Phys. Rev. B **64**, 094510 (2001).
[17] J. M. Tranquada, K. Nakajima, M. Braden, L. Pintschovius, and R. J. McQueeney, Phys. Rev. Lett. **88**, 075505 (2002).
[18] W. Reichardt and M. Braden, Physica B **263**, 416 (1999).
[19] M. Braden, W. Reichardt, A. S. Ivanov, and A. Yu Rumantsiev, Europhys. Lett. **34**, 531 (1996).
[20] M. Braden, W. Reichardt, S. Shiryaev, and S. N. Barilo, eprint arXiv:cond-mat/0107498 (unpublished).
[21] M. Braden, W. Reichardt, S. Shiryaev, and S. Barilo, Physica C **378**, 89 (2002).
[22] S. L. Chaplot, W. Reichardt, L. Pintschovius, and N. Pyka, Phys. Rev. B **52**, 7230 (1995).
[23] P. Brüesch, *Phonons: Theory and Experiments* (Springer-Verlag, Berlin, 1982), Vol. I.
[24] M. Tachiki and S. Takahashi, Phys. Rev. B **39**, 293 (1989).
[25] M. Imada, A. Fujimori, and Y. Tokura, Rev. Mod. Phys. **70**, 1039 (1998).
[26] I. D. Brown and D. Altermatt, Acta Crystallogr., Sect. B: Struct. Sci. **B41**, 244 (1985).
[27] D. Reznik, L. Pintschovius, M. Ito, S. Iikubo, M. Sato, H. Goka, M. Fujita, K. Yamada, G. D. Gu, and J. M. Tranquada, Nature (London) **440**, 1170 (2006).
[28] Y. Maeno, K. Yoshida, H. Hashimoto, S. Nishizaki, S.-I. Ikeda, M. Nohara, T. Fujita, A. P. Mackenzie, N. E. Hussey, J. G.

Bednorz, and F. Lichtenberg, J. Phys. Soc. Jpn. **66**, 1405 (1997).
[29] Y. Sidis, M. Braden, P. Bourges, B. Hennion, S. NishiZaki, Y. Maeno, and Y. Mori, Phys. Rev. Lett. **83**, 3320 (1999).
[30] M. Braden, Y. Sidis, P. Bourges, P. Pfeuty, J. Kulda, Z. Mao, and Y. Maeno, Phys. Rev. B **66**, 064522 (2002).
[31] G. Squires, *Introduction to the Theory of Thermal Neutron Scattering* (Cambridge University Press, Cambridge, 1978).
[32] M. Braden, W. Reichardt, S. Nishizaki, Y. Mori, and Y. Maeno, Phys. Rev. B **57**, 1236 (1998).
[33] M. Braden, G. André, S. Nakatsuji, and Y. Maeno, Phys. Rev. B **58**, 847 (1998).
[34] O. Friedt, M. Braden, G. André, P. Adelmann, S. Nakatsuji, and Y. Maeno, Phys. Rev. B **63**, 174432 (2001).
[35] M. Udagawa, T. Minami, N. Ogita, Y. Maeno, F. Nakamura, T. Fujsita, J. G. Bednorz, and F. Lichtenberg, Physica B **219&220**, 222 (1996).
[36] S. Sakita, S. Nimori, Z. Q. Mao, Y. Maeno, N. Ogita, and M. Udagawa, Phys. Rev. B **63**, 134520 (2001).
[37] T. Katsufuji, M. Kasai, and Y. Tokura, Phys. Rev. Lett. **76**, 126 (1996).
[38] M. Braden, A. H. Moudden, S. Nishizaki, Y. Maeno, and T. Fujita, Physica C **273**, 248 (1997).
[39] W. Reichardt, GENAX-PROGRAM-PACKAGE (unpublished).
[40] N. E. Hussey, A. P. Mackenzie, J. R. Cooper, Y. Maeno, S. Nishizaki, and T. Fujita, Phys. Rev. B **57**, 5505 (1998).
[41] A. W. Tyler, A. P. Mackenzie, S. NishiZaki, and Y. Maeno, Phys. Rev. B **58**, R10107 (1998).
[42] A. Lanzara, P. V. Bogdanov, X. J. Zhou, S. A. Kellar, D. L. Feng, E. D. Lu, T. Yoshida, H. Eisaki, A. Fujimori, K. Kishio, J.-I. Shimoyama, T. Noda, S. Uchida, Z. Hussain, and Z.-X. Shen, Nature (London) **412**, 510 (2001).
[43] S. V. Dordevic, C. C. Homes, J. J. Tu, T. Valla, M. Strongin, P. D. Johnson, G. D. Gu, and D. N. Basov, Phys. Rev. B **71**, 104529 (2005).
[44] Y. Aiura, Y. Yoshida, I. Hase, S. I. Ikeda, M. Higashiguchi, X. Y. Cui, K. Shimada, H. Namatame, M. Taniguchi, and H. Bando, Phys. Rev. Lett. **93**, 117005 (2004).
[45] H. Iwasawa, Y. Aiura, T. Saitoh, I. Hase, S. I. Ikeda, Y. Yoshida, H. Bando, M. Higashiguchi, Y. Miura, X. Y. Cui, K. Shimada, H. Namatame, and M. Taniguchi, Phys. Rev. B **72**, 104514 (2005).
[46] F. Servant, B. Fak, S. Raymond, J. P. Brison, P. Lejay, and J. Flouquet, Phys. Rev. B **65**, 184511 (2002).
[47] C. Falter, M. Klenner, and W. Ludwig, Phys. Rev. B **47**, 5390 (1993).
[48] C. Falter, M. Klenner, and G. A. Hoffmann, Phys. Rev. B **52**, 3702 (1995).
[49] A. F. Ho and A. J. Schofield, Phys. Rev. B **71**, 045101 (2005).
[50] D. F. Agterberg, T. M. Rice, and M. Sigrist, Phys. Rev. Lett. **78**, 3374 (1997).
[51] M. Braden, O. Friedt, Y. Sidis, P. Bourges, M. Minakata, and Y. Maeno, Phys. Rev. Lett. **88**, 197002 (2002).